Continuum Model of Collective Cell Migration in Wound Healing and Colony Expansion

Julia C. Arciero,[†△] Qi Mi,[‡△] Maria F. Branca,[§] David J. Hackam,[§¶‖] and David Swigon[†*]
[†]Department of Mathematics, University of Pittsburgh, Pittsburgh, Pennsylvania; [‡]Department of Sports Medicine and Nutrition, Center for Inflammation and Regenerative Modeling, McGowan Institute for Regenerative Medicine, University of Pittsburgh, Pittsburgh, Pennsylvania; [§]Children's Hospital of Pittsburgh, Division of Pediatric Surgery, University of Pittsburgh, Pittsburgh, Pennsylvania; and [¶]Department of Surgery and [‖]Department of Cell Biology and Physiology, University of Pittsburgh, Pittsburgh, Pennsylvania

ABSTRACT Collective cell migration plays an important role during wound healing and embryo development. Although the exact mechanisms that coordinate such migration are still unknown, experimental studies of moving cell layers have shown that the primary interactions governing the motion of the layer are the force of lamellipodia, the adhesion of cells to the substrate, and the adhesion of cells to each other. Here, we derive a two-dimensional continuum mechanical model of cell-layer migration that is based on a novel assumption of elastic deformation of the layer and incorporates basic mechanical interactions of cells as well as cell proliferation and apoptosis. The evolution equations are solved numerically using a level set method. The model successfully reproduces data from two types of experiments: 1), the contraction of an enterocyte cell layer during wound healing; and 2), the expansion of a radially symmetric colony of MDCK cells, both in the edge migration velocity and in cell-layer density. In accord with experimental observations, and in contrast to reaction-diffusion models, this model predicts a partial wound closure if lamellipod formation is inhibited at the wound edge and gives implications of the effect of spatially restricted proliferation.

INTRODUCTION

Cell migration at the single-cell level has been studied extensively over many decades (1). In brief, each cell moves by a cyclic mechanism that proceeds through stages involving the formation of a lamellipodium, translocation of the nucleus in the direction of motion, and detachment of the trailing edge (2,3). This mechanism is regulated by a complex signaling and regulatory network responsible for the underlying processes of actin polymerization and depolymerization, motor protein activation, and integrin formation and release (1).

Friedl and Gilmour (4) reviewed commonly recognized cellular and molecular mechanisms of collective cell migration and highlighted the distinction between leader cells (located at the wound edge) and follower cells (located in the cell layer) as a typical feature of cell-sheet movement. Both leader and follower cells are observed to develop lamellipodia to coordinate collective migration (5). Farooqui and Fenteany (6) studied wound closure in Madin-Darby canine kidney (MDCK) epithelial cell layers and established that submarginal cells exhibit protrusive and migratory behavior similar to that of marginal cells. The general direction of the coordinated cell movement was toward the wound and the cell velocity within a sheet was found to be inversely proportional to the distance from the wound edge (6). Wound closure was shown to occur even if the motility of edge cells was inhibited, but it occurred at a slower rate (5). Vitorino and Meyer (7) studied growth-factor-induced migration of endothelial cell monolayers and proposed that the growth factor led to directed migration of leader cells but did not control cell migration and coordination of the follower cells.

Mechanically robust and dynamic coupling of cells to one another and to the substrate is accomplished via adherens junction proteins, desmosomal proteins, and integrins (4,8). The cells in the interior are connected to the cells at the boundary by tight junctions, which prevent separation of the cells in the layer (9). The level of adhesion between the cell and the substrate, moderated by integrins, was found to control the speed of wound closure (10). The effects of substrate stiffness on cell traction forces were quantified for epithelial cells and fibroblasts, and it was shown that cell movement could be modulated by changing the stiffness of the substrate (11). Trepat et al. (12) found that traction forces, applied by moving cells on the substrate, were smallest in the center of a cell colony and largest at the edge of the colony of cells moving radially outward. They estimated that tension in the cell layer increased with distance from the edge of the cell colony and argued that accumulated traction stresses were balanced by the forces within the cell sheet; the interplay of these two stresses was described using a tug-of-war model.

In several studies, a release of tension was observed within the cell layer once a wound was induced (13,14). Block et al. (14) compared cell-sheet migration in wounds induced by different methods and hypothesized that the release of spatial constraints initiates a healing response. However, this hypothesis is difficult to verify experimentally since it is

Submitted July 9, 2010, and accepted for publication November 16, 2010.

△Julia C. Arciero and Qi Mi contributed equally to this work.

*Correspondence: swigon@pitt.edu

Editor: Leah Edelstein-Keshet.

0006-3495/11/02/0535/9 $2.00

doi: 10.1016/j.bpj.2010.11.083

hard to eliminate all possible methods (such as biochemical communication) that may contribute to collective cell migration.

Various types of models have been used to test some of these hypotheses and to isolate factors that may direct cell-sheet migration. For example, Bindschadler and McGrath (15) used an agent-based model (ABM) to simulate cell migration in which cells responded to crowded conditions by decreasing their cell division rates and moving to less crowded areas. The model predictions were consistent with experimental rates of closure. Ouaknin and Bar-Yoseph (16) used the Glazier-Graner-Hogeweg (GGH) model to simulate the collective movement of cells, taking into account adhesion energy, deformation energy, and stochastic behavior of the system. The model results were similar to experimental behavior obtained by Poujade et al. (17), in which leader cells progressed faster than the rest of the cell layer and a fingering morphology emerged. Fozard et al. (18) developed an ABM for epithelial monolayers and approximated it by a continuum model in the limit of a large number of cells. Relating agent-based and continuum models may help to estimate model parameters and justify model assumptions. Fozard et al. (18) assumed that the energy dissipation of individual cells was due to the drag between the cell and substrate, as well as the internal viscosity of the cells (which was not accounted for in the model presented here). Active cell migration and cell division were not included in their model, and a more complex formulation of cell-cell and cell-substrate adhesion could provide additional mechanical insight. The continuum model yielded results consistent with the ABM for even a moderate number of cells. Byrne and Drasdo (19) also derived a continuum model from their ABM for the growth of cell aggregates on compact monolayers. Growth was assumed to be governed by contact inhibition, and cells were assumed to proliferate. The continuum model agreed with the ABM in the prediction of initial and asymptotic growth regimes for the radius of the colony and the cell population size.

Existing continuum models of cell migration in wound healing are also often based on reaction-diffusion formalism in which the moving edge of a cell layer is represented as a traveling wave of cell concentration. For adult epidermal wound healing, Sherratt and Murray (20,21) proposed a two-component model in which the epithelial layer is described by the cell density/unit area, and the time dependence of this density is related to the concentration of the mitosis-regulating chemical. For embryonic epidermal wound healing, Sherratt (22) developed a model involving actin filament network formation, based on a mechanochemical model for the deformation of epithelial sheets proposed by Murray and Oster (23). Several studies have modeled wound healing as a free boundary problem to account for the influence of physiological electric fields on wound closure. For example, Gaffney et al. (24) described the evolution of the free boundary problem for a system of two reaction-diffusion equations for cell density and chemical stimulus in the context of corneal wound healing. Chen and Friedman (25) analyzed that model and applied a similar approach to predicting tumor growth (26). Xue et al. (27) developed a continuum model of ischemic dermal wounds with the wound boundary represented as a free boundary that moves with the velocity of the extracellular matrix at the wound edge. The model was used to predict how ischemic conditions may impair wound closure.

We have recently developed a one-dimensional continuum mechanical model of a migrating cell sheet to study the influence of lipopolysaccharide (a protein found in the coat of Gram-negative bacteria) and integrin concentration on wound closure during experimental necrotizing enterocolitis (NEC) (28). The model predicts low migration speed at high and low integrin concentrations and high velocity at medium concentrations, in agreement with experimental observations (10). It also predicts that the edge velocity decreases with time, in accord with our experimental observations but contrary to the behavior of reaction-diffusion models. However, that model is only appropriate to situations in which the wound has a simple geometry with two long parallel wound edges.

In this study, we design a two-dimensional model of cell-layer migration that captures the same primary interactions driving the motion of the cell sheet, namely, the elastic coupling between cells in the layer, the adhesion of cells to the substrate, the force generated by lamellipodia both in the interior and at the wound edge, and the proliferation of cells within the layer, but has the additional benefit of being applicable to an arbitrary wound geometry. The cell sheet is represented as a compressible inviscid fluid, and therefore individual cells are not distinguishable. The leader and follower cells are accounted for in an average manner by including focused traction force applied by the lamellipodia at the edge of the sheet. The two-dimensional character of the problem requires us to use Eulerian independent variables. The physical laws governing the mechanics of the layer then yield a partial differential equation problem with moving boundary that is known as the Stefan problem in other contexts (29,30). The problem is solved numerically using a level set method, and the basic properties of solutions are analyzed. The model is calibrated for two scenarios: the closure of a wound and the expansion of a cell colony. Parameter values in the model are fit to data from a scratch-wound assay as well as to data from a cell colony expanding radially outward (12). Cell proliferation is neglected in wound closure simulations but is included in colony expansion simulations.

THEORY AND METHODS

Mathematical formulation

The cell layer is represented by a two-dimensional compressible fluid, and its configuration is described by giving the density of cells $\rho(x, y, t)$ as a function of the spatial coordinates x and y and time t. This differs from our earlier model (28) which used material coordinates. A relaxed

(unstressed) cell layer is assumed to have a constant density ρ_0. The law of conservation of cell number,

$$\frac{\partial \rho}{\partial t} + \nabla \cdot (\rho \mathbf{v}) = g(\rho), \tag{1}$$

with $\mathbf{v} = (v_x, v_y)$ the velocity of the layer, includes the growth term $g(\rho)$ that describes the density-dependent net rate of change in the number of cells within the layer due to proliferation and apoptosis. In this study, we take $g(\rho) = 0$ when modeling enterocyte migration experiments and assume logistic growth $g(\rho) = \alpha\rho(1 - \rho/\rho_k)$ when modeling cell-colony expansion, where α is the growth rate and ρ_k is the limiting cell density (15). In some cases of MDCK-cell-colony migration, the proliferation appears to be spatially restricted to the site of original location of the cell colony and does not occur in the newly invaded areas (17). In such cases, the growth rate α in $g(\rho)$ is defined as a function of (x, y) that is constant at the original colony location Ω^0 (see Fig. 1) and zero otherwise.

In the law of the balance of linear momentum,

$$\rho \frac{\partial \mathbf{v}}{\partial t} + \rho(\mathbf{v} \cdot \nabla)\mathbf{v} = \mathbf{f} + \nabla \cdot \mathbf{T}, \tag{2}$$

the force $\mathbf{f}$ accounts for the force of adhesion of the cell layer to the substrate, and the tensor $\mathbf{T}$ represents the stresses within the sheet. (Traditional body forces, such as gravity or electrostatic force, are expressed as force/unit density, but that is not necessary for the interactions considered here.)

The force $\mathbf{f}$ is the result of the action exerted on a material element by the substrate, i.e., the negative of traction force. It is assumed to be negatively proportional to the layer velocity,

$$\mathbf{f} = -b\mathbf{v}, \tag{3}$$

where b is an adhesion constant. The cell layer is assumed to behave as a compressible inviscid fluid with the constitutive equation

$$\mathbf{T} = -p(\rho)\mathrm{I}, \tag{4}$$

where p, the pressure within the layer, depends on the cell density and is taken to be positive when cells are compressed and negative when cells are stretched.

The acceleration of each individual cell is assumed to be negligible compared to its velocity, and thus, the material time derivative of the velocity, $\rho\mathbf{v}$ (i.e., the lefthand side of Eq. 2), can be neglected, which, in view of Eqs. 3 and 4 gives the following relation between the velocity of cells and the gradient of cell density:

$$b\mathbf{v} = -p'(\rho)\nabla\rho \tag{5}$$

Equation 5 resembles the familiar Darcy's law describing the flow of a fluid through a porous medium. Substituting the result into Eq. 1 implies that the evolution of cell density is governed by a nonlinear parabolic equation:

$$\frac{\partial \rho}{\partial t} = \frac{1}{b}\nabla \cdot (\rho p'(\rho)\nabla\rho) + g(\rho) \tag{6}$$

We have considered several choices for the dependence of p on ρ. Unlike Hooke's Law, $p(\rho) = k(1 - (\rho_0/\rho))$, or the Ideal Gas Law, $p(\rho) = k((\rho/\rho_0) - 1)$, the relation

$$p(\rho) = k \ln(\rho/\rho_0) \tag{7}$$

gives an appropriate behavior at both large and small densities, since it allows for an infinite magnitude of stress for both infinite stretch and compression. Although it is known that any deformation of a cell is accompanied by an active remodeling of the cytoskeleton, which results in a viscoelastic stress-strain response (31), the timescale of the collective motion of the layer (order of hours) is slow compared to the relaxation time of single-cell deformation, which is of the order of tens of seconds (32). Thus, our choice of a constitutive equation for $\mathbf{T}$ implicitly assumes that the cell layer responds instantaneously and passively to the forces generated on it, and that one should treat k as the residual bulk modulus of the layer after cytoskeleton relaxation.

The constitutive relation Eq. 7 gives the following form of the governing Eq. 6:

$$\frac{\partial \rho}{\partial t} = \kappa\Delta\rho + g(\rho), \tag{8}$$

where $\kappa = k/b$. (Note that the appearance of the Laplacian in Eq. 8 is a result of our choice of the constitutive equation and does not arise from any underlying diffusion process or Brownian motion; in particular, κ should not be interpreted as a diffusion coefficient.)

The partial differential equation in Eq. 8 is assumed to hold in the interior of the domain Ω^t that describes the extent of the cell sheet at time t, as in Fig. 1, *A* or *B*. The BCs will be defined in terms of the wound-closure scenario, Fig. 1 *A*, but it is straightforward to transform the problem into one describing expansion of a cell colony, as depicted in Fig. 1 *B*. The initial domain Ω^t covered by the cell layer has the topology of an annulus with an inner boundary $\partial\Omega_1^t$ and an outer boundary $\partial\Omega_2$ (see Fig. 1 *A*).

The initial density of the layer depends on the situation studied. For simulations reported in this study, we have assumed $\rho(x, 0)$ to be constant. In wound-healing simulations (as in Figs. 2 and 3 below), the initial density reflects the amount of prestress in the layer generated by lamellipod action in the interior of the sheet when grown to confluence. At rest, the lamellipodia exert a pressure (force/unit length) F on neighboring cells and hence, in view of the constitutive equation, $\rho(x, 0) = e^{\phi}\rho_0$, where $\phi = F/k$. In addition, to avoid a discontinuity at the wound edge, a smoothing function is applied at a narrow band (1 μm) surrounding the wound edge. (The form of the smoothing does not significantly affect model predictions.) In simulations of colony expansion, the initial colony may be seeded with a small density. For such cases (as in Fig. 4) it is appropriate to assume that the initial density is equal to the density of a stretched layer, $\rho(x, 0) = e^{-\phi}\rho_0$.

The conditions at the outer boundary $\partial\Omega_2$ represent two cases: 1), the edge of the coverslip region; and 2), the edge of the observable region in the experiment. In the first case, there is no flux of cells across the boundary, which leads to the Neumann BC. In the second case, it is assumed that there is a constant source of cells beyond the boundary capable of maintaining constant density at the boundary, resulting in the Dirichlet (BC):

$$\text{Neumann BC}: \nabla\rho \cdot \mathbf{n} = 0 \; on \; \partial\Omega_2; \tag{9}$$

$$\text{Dirichlet BC}: \rho = e^{\phi}\rho_0 \text{ on } \partial\Omega_2. \tag{10}$$

The inner boundary $\partial\Omega_1^t$ represents the wound edge, and, as the notation suggests, its location depends on time. The lamellipodia at the wound edge exert a constant force/unit length, F, at the wound edge that is equal in magnitude to that of cells in the interior, and hence the appropriate boundary condition is of Dirichlet type

$$\rho = e^{-\phi}\rho_0 \text{ on } \partial\Omega_1^t. \tag{11}$$

An additional boundary condition describing the speed of the moving edge is given by Eq. 5, which, in combination with Eqs. 7 and 11, implies that

$$\mathbf{v} = -\kappa e^{\phi}\rho_0^{-1}\nabla\rho \text{ on } \partial\Omega_1^t. \tag{12}$$

This reduces to the Stefan condition,

$$\mathbf{v} \cdot \mathbf{n} = -\kappa e^{\phi}\rho_0^{-1}\nabla\rho \cdot \mathbf{n} \text{ on } \partial\Omega_1^t, \tag{13}$$

where $\mathbf{n}$ is the unit outward normal to $\partial\Omega_1^t$ (here pointing into the wound).

The free-boundary problem characterized by Eq. 8 (with $g = 0$) and BCs in Eqs. 9–11 and 13 is known as the Stefan problem. The Stefan problem

was first derived for the transfer of heat during solidification or melting processes with ρ representing the temperature and $\partial\Omega_1^t$ the phase boundary. The Stefan problem has been extensively studied in many contexts: short-time existence of classical solutions for smooth domains was shown by Hanzawa (33), and global existence and uniqueness of weak solutions were shown by Kamenomostskaja (34), Oleinik (35), and Friedman (36). It is known that negative values of F (opposite of the present case) give rise to Mullins-Sekerka instability in boundary motion, which leads to a loss of regularity and fingering (37).

To understand the difference between the behavior of this model and a much simpler diffusion equation model consisting of Eq. 8 with no free boundary, consider the case with the Neumann BC applied at $\partial\Omega_2$ and no proliferation. In both models the total amount, P, of cells is conserved. If the area, A, of the region to be covered (which equals Ω^0 plus the area of the wound) is $<P/(\rho_0 e^{-\phi})$, then the limiting equilibrium state will be the same in both models: a constant density $\rho = P/A$. However, if $A > P/(\rho_0 e^{-\phi})$, then this model will converge to a state in which the migration of the edge will stop before the hole is completely closed, because the equilibrium density in the current model is $\rho_0 e^{-\phi}$, as determined by the Dirichlet condition on Ω_1^t. The diffusion equation model will predict closure of the wound no matter what its area, because the diffusion model is in equilibrium at any constant density. This is clearly unrealistic, as a finite number of cells cannot cover an arbitrarily large area. A similar issue arises in cell-colony expansion if proliferation is inhibited.

A careful examination of Eqs. 8–11 and 13 reveals that the model is characterized by two reduced material constants, κ and ϕ; a scaling factor, ρ_0; and, if growth is considered, the growth rate, α. The constant ϕ has dimensionless units, whereas κ has the units of length squared over time. In view of Eqs. 8 and 13, any change in κ can be compensated for by a change in the timescale. The limiting density ρ_k will be assumed equal to $\rho_0 e^{\phi}$.

Experimental Setup

The continuum mechanical model of natural cell migration developed in this study is applied to two sets of experimental data. In the first, which was obtained in the Hackam Lab at the University of Pittsburgh, small intestinal enterocytes (IEC-6 cells) were cultured on a glass coverslip, grown to 100% confluence, serum-starved for 12 h, and then scraped with a pipette or cell scraper to create a gap that represents the wound (scratch wound assay). The slide was mounted on the stage of an IX81 Olympus Livecell (Tokyo, Japan) inverted microscope warmed to 37°C. Fresh medium was continuously perfused across the cells. The enterocyte cell layer is one cell thick, and the motion and deformation of cells in the layer were captured at 5-min intervals using differential interference contrast imaging.

For the second case, we use published data of Trepat et al. (12), who studied the migration of a colony of MDCK cells plated on a soft collagen-coated polyacrylamide gel. The colony was seeded and grown to confluence for 24 h. The colony expanded radially with time, and the growth of the colony was observed to be insensitive to the stiffness of the underlying substrate.

Optimization of parameter values

A numerical solution of the Stefan problem for a given wound geometry and parameters ϕ, κ, and ρ_0 is found using a level set method introduced by Osher and Sethian (38) and applied to Stefan problems by Chen et al. (39), Javierre et al. (40), and others. Please see the Supporting Material for details of the solution method. Optimal values of ϕ, κ, and ρ_0 are found by minimizing the sum of the mean-squared difference between the experimental and predicted cell-density values and the mean-squared difference between the experimental and predicted wound-edge positions.

In calibrations of the wound-closure experiment, density data are extracted from movies of cell migration for wounds of various initial shapes. The experimental tissue domain is divided into 192 subregions of dimensions 3.125 μm × 3.175 μm, and the cell centers (c) within each subregion are counted. The number of cell centers is divided by the area of the subregion (A) to compute the experimental cell density: $\rho_{exp} = c/A$. Experimental density values are compared with the model-predicted values of cell density interpolated at the center of each subregion.

The square root of the average of the squares of the differences between the experimental cell density and model-predicted cell density (ρ_{comp}) is calculated and denoted as ρ_{rms}:

$$\rho_{rms,\,j} = \sqrt{\sum_{i=1}^{n} \frac{\left(\rho_{exp,i} - \rho_{comp,i}\right)^2}{n}}, \tag{14}$$

where index i denotes the subregion at which density is computed, n is the total number of subregions, and index j denotes the hourly time point at which $\rho_{rms,j}$ is calculated. Let t_{end} denote the total number of time points at which density is measured. Summing over all time points gives

$$z_\rho = \sum_{j=1}^{t_{end}} \rho_{rms,\,j}. \tag{15}$$

The positions of the wound edge corresponding to 1-h intervals of a given experiment are extracted from the microscope image by eye, with error expected to be smaller than one-fifth of the cell width. Approximately 1 point/5 cells is used to define the edge. To calculate the difference between experimental and computational wound-edge positions, the minimum distance from every experimental point to every line segment along the computational wound edge is found at time intervals of 1 h and denoted $d_{min,j}$. The square root of the average of the squares of these minimum distances is calculated and denoted d_{rms}:

$$d_{rms,\,j} = \sqrt{\sum_{h=1}^{m} \frac{d_{min,\,j}^2}{m}}, \tag{16}$$

where index h denotes the experimental points counted along the edge of the wound and m is the total number of these points. Summing over all time points gives

$$z_d = \sum_{j=1}^{t_{end}} d_{rms,\,j}. \tag{17}$$

To optimize according to both cell density and wound-edge position, we minimize the value of $z = z_\rho + z_d$.

In calibration to MDCK cell migration experiments, we use data for the density of cells as a function of distance from the leading cell edge and the radius of the cell colony at 24-h time intervals reported in the supporting materials of Trepat et al. (12). The model is adapted to allow for logistic proliferation. Optimized values of ϕ, κ, and α are found by minimizing the mean-squared difference between experimental and computed cell densities and colony radii. The squared difference of experimental and predicted colony radii is multiplied by a weighting factor of 10^8.

RESULTS

Enterocyte migration during wound healing

In the scratch-wound assays we performed with IEC-6 cells, apoptosis is observed to be approximately balanced by proliferation, and therefore, we assume no net growth in the layer, i.e., $g = 0$ in Eq. 8. The computational domain is taken to be the observed area minus the initial location of the wound (Fig. 1 *A*). By fitting the predicted density of the cell sheet and the wound-edge position with available data we obtained the following values for the constants of the model:

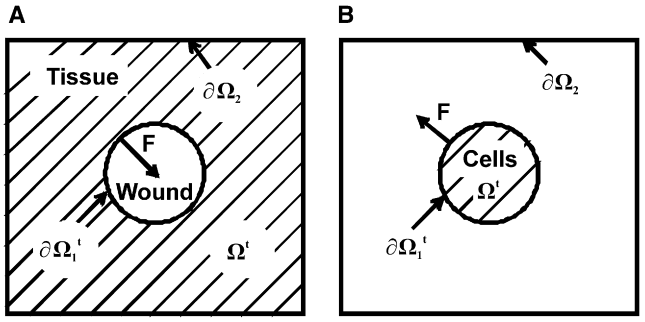

FIGURE 1 Computational domain of the moving boundary initial value problem. (*A*) Schematic of the tissue layer and scratch wound. The hatched area (Ωt) represents the cell layer, and the white area is a cell-free region. Two boundaries of Ωt are labeled $\partial\Omega_1^t$ (wound edge) and $\partial\Omega_2^t$ (exterior tissue edge). F is the force exerted by cells at the wound edge. (*B*) Schematic of radially symmetric cell colony (Ωt, *hatched area*). Two boundaries of Ωt are labeled $\partial\Omega_1^t$ (cell-colony edge) and $\partial\Omega_2^t$ (outer boundary of viewing area). F is the force exerted by cells at the colony edge.

$$\phi = 0.191, \kappa = 73.33\mu\text{m}^2/\text{h}, \rho_0 = 0.604\text{cells}/\mu\text{m}^2 \tag{18}$$

Fig. 2 shows the predicted locations of two different wound edges (*yellow lines*) overlaid on the experimental images. Black dots denote the experimental wound edge, which is taken to be the edge of the lamellipodia of boundary cells and is not easily visible at the resolution shown in the figure. Fig. 2, *A–E* and *J*, shows an example of parameter calibration for an experimental wound (wound 1). Fig. 2 *E* gives the relative difference ($\Delta\rho$) between experimental and model-predicted cell densities normalized by the initial density, ρ_0, for wound 1 at time $t = 6$ h (near full wound closure). The difference $\Delta\rho$ is estimated in 192 subregions of tissue, and is observed to have a random spatial distribution. The histogram in Fig. 2 *J* shows that the distribution of the magnitude of $\Delta\rho$ is close to normal.

Fig. 2, *F–I*, shows an example of a validation of the parameter fit. Since the conditions and cell types were the same for experimental wound 2 (Fig. 2 *F*) as for wound 1, we validate the fit by predicting the closure of a wound of different geometry, depicted in Fig. 2, *F–I*, using parameter values optimized for wound 1. We found that a single wound-closure experiment provides a sufficient amount of data for estimation of all parameters in the model and that the prediction of the model is consistent with experimental results.

In several experimental studies, wound closure has been observed to occur even if lamellipod formation at the wound edge is inhibited (5,17). This behavior can be demonstrated in our continuum mechanical model by regulating the driving force of boundary lamellipodia (Fig. 3). Under normal conditions, lamellipodia are assumed to form at the wound edge, and thus, the initial density at the wound edge is given by $\rho = \rho_0 e^{-\Phi}$ on $\partial\Omega_1^0$. To block lamellipodia formation at the wound edge, we set $F = 0$ on $\partial\Omega_1^0$ (and thus $\Phi = F/k = 0$). Thus, when lamellipodia are inhibited on the edge, the initial density is given by $\rho = \rho_0$ on $\partial\Omega_1^0$.

If lamellipodia are assumed to form at the edge, the wound is completely closed in slightly more than 3 h (Fig. 3 *A*). If lamellipodia formation at the wound edge is inhibited, the closure of the wound proceeds at a much slower pace (Fig. 3 *B*), since migration is driven only by the lamellipod formation within the interior of the sheet.

MDCK-cell-colony expansion

Colonies of MDCK cells expand from an initial seed location due to migration and proliferation. Trepat et al. (12) measured the expansion of an MDCK cell colony by

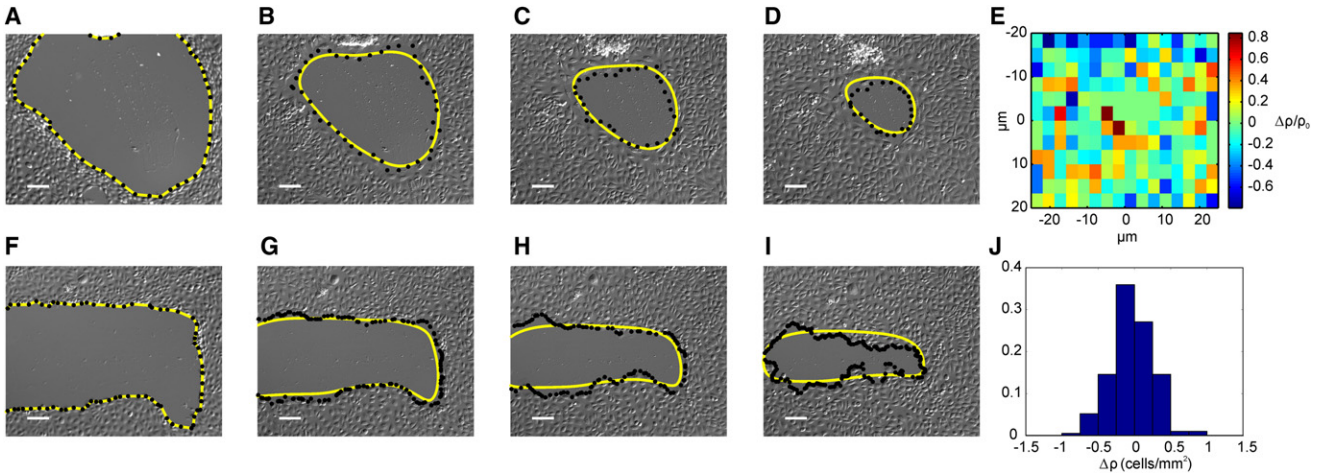

FIGURE 2 Comparison of model predictions (*yellow lines*) with experimental wound closure, represented as the experimental edge (*black dotted lines*). (*A–D*): Progression of experimental wound 1 at 2-h time intervals ($t = 0$, 2, 4, and 6 h). Optimized parameter values from wound 1 are $\phi = 0.191$, $\kappa = 73.33\ \mu\text{m}^2/\text{h}$, and $\rho_0 = 0.604$ cells/μm^2 with Dirichlet BCs imposed at the outer boundary. (*E*) The difference between model-predicted and experimental cell density $\Delta\rho$ normalized by ρ_0 is shown for wound 1 at $t = 6$ h. (*F–I*) Progression of experimental wound 2 at 1-h time intervals ($t = 0$, 1, 2, and 3 h) using the parameter values estimated for wound 1. (*J*) Histogram of differences in predicted and experimental density for wound #1 at $t = 6$ h. The vertical axis indicates the percentage of total grid boxes where $\Delta\rho$ takes on a particular value. The images are 1344 × 1024 pixels. Scale bar, 5 μm.

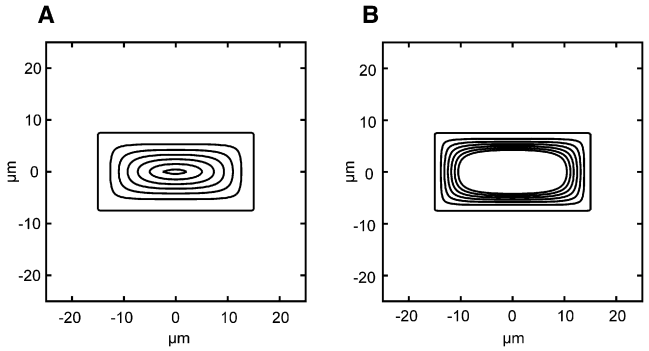

FIGURE 3 Effect on wound closure of the neutralization of lamellipod formation at the wound edge. (*A*) Regular migration, including the force of lamellipodia at the wound edge as well as in the interior of the cell layer. (*B*) Migration with neutralized formation of edge lamellipodia. Initial wound dimension is 30 μm × 15 μm; the evolution is shown for 3 h at 0.5-h intervals. In the case of regular migration (*A*), the wound closes completely. Parameters are as in Fig. 2.

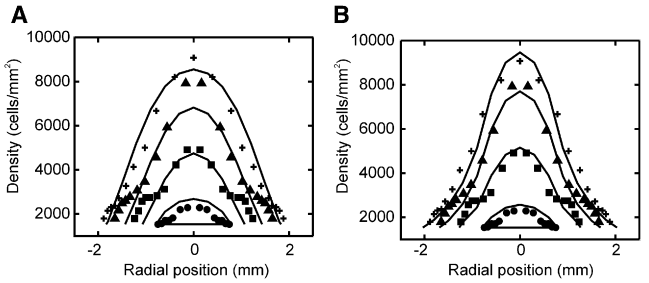

FIGURE 4 Prediction of cell density in an expanding MDCK colony. (*A*) Spatially independent proliferation model. (*B*) Model with proliferation limited to the initial colony location. Experimental densities measured by Trepat et al. (12) at equally spaced time points: t = 24 h (*circles*), 48 h (*squares*), 72 h (*triangles*), and 96 h (*plus signs*). Optimal fit parameters are (*A*) $\phi = 0.971$, $\kappa = 5000\ \mu\text{m}^2/\text{h}$, $\alpha = 0.0580\ \text{h}^{-1}$, $\rho_0 = 0.004046$ cells/μm^2 and (B) $\phi = 1.158$, $\kappa = 13{,}700\mu\text{m}^2/\text{h}$, $\alpha = 0.0913\ \text{h}^{-1}$, and $\rho_0 = 0.004876$ cells/μm^2. The colony is circular with initial radius 787 μm and initial cell density constant (*thin solid line*). The cell colony is centered about zero on the horizontal axis, and the distance from the vertical axis to the edge of each curve corresponds to the average radius of the colony at each time point.

recording the cell density as a function of distance from the leading edge of the cell layer at 24-h time intervals. Since colony expansion is observed over a much longer time period than wound closure (96 h versus 6 h), growth of the layer plays a prominent role and is included explicitly in Eq. 1 as a logistic term. Poujade et al. (17) observed that cell proliferation by a colony of MDCK cells occurred almost exclusively within the band where cells were originally seeded and not in the area into which the cells had migrated. They speculate that this is likely due to the longer presence of cells in the originally seeded region or modifications made by cells to the underlying substrate that promote cell divisions (17). In the study by Trepat et al. (12), it is not known whether the proliferation in the layer was spatially restricted or not, and therefore we explore both possibilities. By fitting predicted density of the cell colony with available data we obtained the following values for the constants of the model with spatially uniform proliferation,

$$\begin{aligned}&\phi = 0.971, \kappa = 5000\ \mu\text{m}^2/\text{h}, \alpha = 0.0580\text{h}^{-1},\\ &\rho_0 = 0.004046\text{cells}/\mu\text{m}^2,\end{aligned} \tag{19}$$

and with proliferation constrained to the original location of the colony:

$$\begin{aligned}&\phi = 1.158, \kappa = 13700\mu m^2/\text{h}, \alpha = 0.0913h^{-1},\\ &\rho_0 = 0.004876\ \text{cells}/\mu m^2.\end{aligned} \tag{20}$$

The optimized parameter values are larger for spatially limited proliferation than for constant proliferation. Comparisons of model predictions and available data are shown in Fig. 4, *A* and *B*, for the assumption of spatially uniform proliferation and spatially restricted growth, respectively. As Fig. 4 makes clear, the assumption of spatially limited proliferation fits the data with much higher accuracy—the density profile assumes a characteristic bell-shaped curve that increases more rapidly in height than in width, until the limiting population density ρ_k is reached. The unlimited-growth case exhibits a parabolic density profile.

Several techniques have been implemented for placing or removing cells along a specified geometry as an alternative to scraping. One example is a procedure in which a microstencil with long rectangular openings is deposited on a surface and cells are plated in the openings and cultured until they reach confluence (17). At that point, the stencils are removed and cell migration is observed. We used our model to investigate the migration of cells originating in two long rectangular regions (Fig. 5). As in Fig. 4, we consider two types of proliferation: a spatially constant proliferation rate (see Fig. 5, *A* and *B*) or spatially restricted proliferation, where growth occurs only within the original rectangular region of cells (see Fig. 5, *C* and *D*). In Fig. 5, *A* and *C*, each rectangular region is initially 400 μm wide and 2800 μm long, and the rectangles are located 400 μm from each other. In Fig. 5, *B* and *D*, the position of the rightmost edge of cells is plotted against time for rectangles of widths 150, 200, 250, 300, 350, and 400 μm. Colony-edge expansion can be fitted by a power law $x \sim t^n$, with $n = 1.29 \pm 0.05$ for unrestricted growth and $n = 1.02 \pm 0.02$ for spatially restricted growth. Our results differ from the experimental growth reported by Poujade et al. (17), which obeys a power law with exponent $n = 1.8 \pm 0.4$. The difference between our estimates may be due to the difference in stiffness of the underlying substrate.

DISCUSSION

We present a two-dimensional continuum model of cell-sheet migration that is based on mechanical principles governing the motion of the sheet, such as the force of lamellipodia, adhesion of cells to the substrate, elasticity of the cell sheet, and the growth of the layer. This enables one to compare the predictions of the model directly with

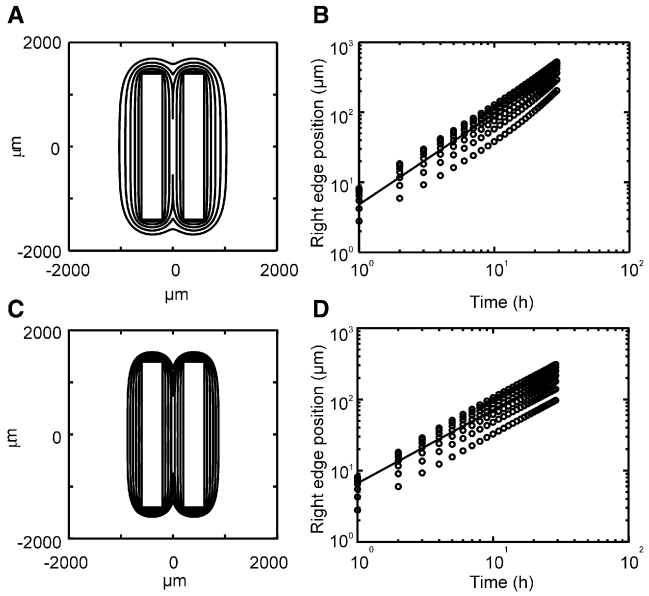

FIGURE 5 Dependence of colony expansion speed on the mode of proliferation: (*A* and *B*) Proliferation rate is assumed constant throughout the expanding layer. (*C* and *D*) Proliferation is spatially restricted to the initial colony location. In *A* and *C*, the initial colony is located in the two rectangular regions of dimensions 400 μm $\times$ 2800 μm, and progression of the colony edge is shown in 5-h increments. In *B* and *D*, the location of the rightmost edge of the colony is plotted for initial rectangles of widths 400 (*upper circles*), 350, 300, 250, 200, 150, and 100 μm (*lowest circles*). Power law fit is indicated by the solid line $x = at^n$ with $n = 1.29 \pm 0.05$ (*B*) and $n = 1.02 \pm 0.02$ (*D*). Parameter values are as in Fig. 4.

mechanical measurements of traction forces and brings the modeling approach into closer alignment with current knowledge of cell-sheet dynamics and the latest developments in cell biomechanics. The model captures the known quantitative and qualitative features of a migrating cell layer, including slowed wound closure when edge lamellipod formation is inhibited (6,5). For both wound healing and cell-colony expansion situations, the calibrated model accurately predicts the edge velocity and shape and the density of cells within the layer.

One surprising finding is that the parameters governing the motion of the layer differ significantly among cell types. The IEC-6 cells have 10-fold lower ϕ and 100-fold lower κ compared to the MDCK cells. This implies that the ratio of the lamellipod force to the adhesion coefficient, $F/b = \phi\kappa$, is 3 orders of magnitude larger for MDCK than for IEC-6 cells. One reason could be that the MDCK cells are much larger. In the stress-free configuration, one MDCK cell has a diameter of ~16 μm, whereas an IEC-6 cell in the same situation has a diameter of ~1.4 μm. It is possible that a large cell is capable of generating stronger lamellipod forces while the total adhesion strength of the cell stays constant, implying that parameter b is smaller for a larger cell than for a smaller cell.

The nature of the model allows us to estimate only the ratios of quantities of interest (κ represents the ratio of the bulk modulus of layer k to adhesion coefficient b, whereas ϕ is the ratio of force F exerted by lamellipodia to bulk modulus k). To obtain true magnitudes of F, b, and k, one needs to perform an independent measurement of at least one of these quantities. The most easily measurable quantity is force. For example, Du Roure et al. (41) measured the force applied by MDCK cells onto elastomeric microfabricated pillars and found average traction stresses of 1.6 nN/μm^2 within a distance of 2 μm from the edge, corresponding to $F = 3.2$ nN/μm. If the cells migrating in the experiments we study exert a similar force, then the corresponding bulk modulus k is 2.76 nN/μm and adhesion coefficient b is 0.0002 nNh/μm^3.

Although many of the physical assumptions underlying this model are the same ones used for our one-dimensional model (28), the model presented here is fundamentally different. The jump to two dimensions requires new assumptions about the fluidity, plasticity, and viscosity of the medium that are not required in a one-dimensional setting. In addition, this model is based on a spatial (Eulerian) description of the problem, and because it includes a free boundary, it is solved using an advanced numerical method (i.e., the level-set method) that accounts for a deforming boundary of the computational domain. The model no longer requires simplifying assumptions about the shape of the wound, but is applicable to wounds of any size and shape. It provides a means of investigating how factors such as the density of the cell layer and boundary conditions of the tissue domain affect wound closure. Also, the parameter values governing the model behavior have a different interpretation in the two-dimensional context. For example, the normal velocity of the wound edge is regulated by $\phi = F/k$, and since this value increases as the force at the edge of the wound increases, it thus will affect both the timing and shape of the wound edge as cells migrate inward.

To describe the migration of a monolayer, some recent studies (19,18) have used a continuum model built on mechanistic principles similar to those of our models; in fact, the model in Mi et al. (28) can be considered a special instance of the model presented in Fozard et al. (18). The latter is focused primarily on the derivation of continuum models from discrete cell representations, whereas the former model is presented with the constitutive assumption of cell density, which was chosen based on agent-based model results from the same authors. The distinguishing feature of the model described here is the choice of a constitutive equation that leads to a classical Stefan problem formulation with a moving boundary representing the wound edge (or cell-colony edge). By fitting a large quantity of experimental data in future studies one may obtain an improved constitutive relation that could provide additional details about the cell-layer mechanics. The ability of the model to predict wound-closure times for complex initial wound geometries, including those that lead to a change in wound topology, could be of great benefit in medical applications.

When applied to a wound-healing scenario, this model predicts a velocity of wound closure that is consistent with experimental observations (Fig. 2). This velocity is high initially, then decreases and remains essentially constant during the entire healing process. In some experimental situations, there may be a short delay in communicating the initial presence of a wound to the surrounding cells. In addition, scratching of a monolayer may yield a transient disruption in the interactions between cells and the surface (17). These explanations may partially account for the slight difference between the experimental and predicted closing rates observed during the initial stages of closure. In addition, there are differences between experimental and predicted wound shapes and densities that are due to the randomness of cell motion, which is to be expected—it is akin to thermal fluctuations in studies of macromolecular assemblies. Although the optimized parameters give a satisfactory fit between model predictions and experimental results, once additional data are available, the best fit over a larger ensemble of initial geometries in the two-dimensional case could be computed to determine optimal values for ϕ, κ, and ρ_0.

When applied to a cell-colony scenario, the model predicts an increase in cell density (and stress) when approaching the center of the cell colony. A shoulder is observed in the experimental observations of cell density at various distances from the colony edge in the study by Trepat et al. (12). This phenomenon does not show up in our model prediction; it may be caused by variable conditions at the experimental surface. Again the model predictions should be thought of as averaging over the inhomogeneities observed experimentally. Our results suggest that in the experiments of Trepat et al. (12), as in those of Poujade et al. (17), the cells proliferate only in the region originally seeded by the cells.

In both scenarios, the model parameters are fit to experimental data that give the position of the edge and the density of the cell layer. Using these two types of data allows the model to capture more accurately the details of the migrating layer. The difference in optimized parameters for the wound-healing and cell-expansion scenarios is likely due to the difference in cell type and experimental protocol. The intestinal epithelial cells were plated on a glass coverslip in the wound-healing scenario, whereas canine kidney epithelial cells were plated on a soft collagen-coated polyacrylamide gel. Studies have shown that different substrates primarily affect cell migration.

As in Poujade et al. (17), this model predicts that the migration of cells originating within a rectangular region will be independent of the initial width of the rectangle (see Fig. 5) provided that the width is >150 μm. If the initial rectangle is 100 μm, the progression is observed to speed up, which is in contrast to the findings of Poujade et al. (17). The difference between our estimates and the results of those experiments (17) can be contributed to the stiffness of the underlying substrate. Specifically, in our experiments, and in experiments by Trepat et al. (12), a glass coverslip coated with fibronectin was used, whereas Poujade et al. (17) used soft polyacrylamide gel.

In contrast to agent-based models, which aim to include several individual cell behaviors and processes, the biophysical model presented here subsumes the details of the chemical regulation of cell migration into three parameters, ϕ, κ, and α, representing ratios of three physical constants and the proliferation rate. The advantage of this approach is that the parameters can be fit easily and with good accuracy even from a limited amount of experimental data. It is important to point out that after calibration, the model can be used to elucidate the influence of experimental conditions or gene knockouts on the mechanical interactions governing the migration of the cell layer, namely, the strength of lamellipod force, strength of adhesion, and the elasticity of the sheet. The use of a continuum model is appropriate as long as the characteristic length of the wound is several times larger than the size of a cell (42). Likewise, any geometrical features of the wound edge can be accounted for in the continuum model provided that the wavelength (mean size) of such features is several times larger than the cell size. Once the wound approaches the closure point, discrepancies between continuum model prediction and reality may arise. We plan to investigate such discrepancies using agent-based models.

SUPPORTING MATERIAL

Numerical method is available at http://www.biophysj.org/biophysj/supplemental/S0006-3495(10)05192-1.

The authors thank Etelvina Javierre and Fred Vermolen for sharing their finite difference code for solving the Stefan problem.

J.C.A. acknowledges support from the National Science Foundation (grant EMSW21-RTG 0739261). Q.M. acknowledges grant support from the National Institute on Disability and Rehabilitation Research (H133 E0700249) and the National Institutes of Health (P50-GM-53789-08). D.J.H. acknowledges support from the National Institutes of Health (R01 GM8238-01). D.S. acknowledges support from an Alfred P. Sloan Fellowship.

REFERENCES

1. Ridley, A. J., M. A. Schwartz, …, A. R. Horwitz. 2003. Cell migration: integrating signals from front to back. *Science.* 302:1704–1709.
2. Mogilner, A. 2009. Mathematics of cell motility: have we got its number? *J. Math. Biol.* 58:105–134.
3. Lauffenburger, D. A., and A. F. Horwitz. 1996. Cell migration: a physically integrated molecular process. *Cell.* 84:359–369.
4. Friedl, P., and D. Gilmour. 2009. Collective cell migration in morphogenesis, regeneration and cancer. *Nat. Rev. Mol. Cell Biol.* 10:445–457.
5. Fenteany, G., P. A. Janmey, and T. P. Stossel. 2000. Signaling pathways and cell mechanics involved in wound closure by epithelial cell sheets. *Curr. Biol.* 10:831–838.
6. Farooqui, R., and G. Fenteany. 2005. Multiple rows of cells behind an epithelial wound edge extend cryptic lamellipodia to collectively drive cell-sheet movement. *J. Cell Sci.* 118:51–63.

7. Vitorino, P., and T. Meyer. 2008. Modular control of endothelial sheet migration. *Genes Dev.* 22:3268–3281.
8. Ilina, O., and P. Friedl. 2009. Mechanisms of collective cell migration at a glance. *J. Cell Sci.* 122:3203–3208.
9. Anand, R. J., C. L. Leaphart, …, D. J. Hackam. 2007. The role of the intestinal barrier in the pathogenesis of necrotizing enterocolitis. *Shock.* 27:124–133.
10. Palecek, S. P., J. C. Loftus, …, A. F. Horwitz. 1997. Integrin-ligand binding properties govern cell migration speed through cell-substratum adhesiveness. *Nature.* 385:537–540.
11. Ghibaudo, M., A. Saez, …, B. Ladoux. 2008. Traction forces and rigidity sensing regulate cell functions. *Soft Matter.* 4:1836–1843.
12. Trepat, X., M. R. Wasserman, …, J. J. Fredberg. 2009. Physical forces during collective cell migration. *Nat. Phys.* 5:426–430.
13. Jacinto, A., A. Martinez-Arias, and P. Martin. 2001. Mechanisms of epithelial fusion and repair. *Nat. Cell Biol.* 3:E117–E123.
14. Block, E. R., A. R. Matela, …, J. K. Klarlund. 2004. Wounding induces motility in sheets of corneal epithelial cells through loss of spatial constraints: role of heparin-binding epidermal growth factor-like growth factor signaling. *J. Biol. Chem.* 279:24307–24312.
15. Bindschadler, M., and J. L. McGrath. 2007. Sheet migration by wounded monolayers as an emergent property of single-cell dynamics. *J. Cell Sci.* 120:876–884.
16. Ouaknin, G. Y., and P. Z. Bar-Yoseph. 2009. Stochastic collective movement of cells and fingering morphology: no maverick cells. *Biophys. J.* 97:1811–1821.
17. Poujade, M., E. Grasland-Mongrain, …, P. Silberzan. 2007. Collective migration of an epithelial monolayer in response to a model wound. *Proc. Natl. Acad. Sci. USA.* 104:15988–15993.
18. Fozard, J. A., H. M. Byrne, …, J. R. King. 2010. Continuum approximations of individual-based models for epithelial monolayers. *Math. Med. Biol.* 27:39–74.
19. Byrne, H., and D. Drasdo. 2009. Individual-based and continuum models of growing cell populations: a comparison. *J. Math. Biol.* 58:657–687.
20. Sherratt, J. A., and J. D. Murray. 1990. Models of epidermal wound healing. *Proc. Biol. Sci.* 241:29–36.
21. Sherratt, J. A., and J. D. Murray. 1991. Mathematical analysis of a basic model for epidermal wound healing. *J. Math. Biol.* 29:389–404.
22. Sherratt, J. A. 1993. Actin aggregation and embryonic epidermal wound healing. *J. Math. Biol.* 31:703–716.
23. Murray, J. D., and G. F. Oster. 1984. Generation of biological pattern and form. *IMA J. Math. Appl. Med. Biol.* 1:51–75.
24. Gaffney, E. A., P. K. Maini, …, J. V. Forrester. 1999. Modelling corneal epithelial wound closure in the presence of physiological electric fields via a moving boundary formalism. *IMA J. Math. Appl. Med. Biol.* 16:369–393.
25. Chen, X., and A. Friedman. 2000. A free boundary problem arising in a model of wound healing. *SIAM J. Math. Anal.* 32:778–800.
26. Chen, X., and A. Friedman. 2003. A free boundary problem for an elliptic-hyperbolic system: an application to tumor growth. *SIAM J. Math. Anal.* 35:974–986.
27. Xue, C., A. Friedman, and C. K. Sen. 2009. A mathematical model of ischemic cutaneous wounds. *Proc. Natl. Acad. Sci. USA.* 106:16782–16787.
28. Mi, Q., D. Swigon, …, D. J. Hackam. 2007. One-dimensional elastic continuum model of enterocyte layer migration. *Biophys. J.* 93:3745–3752.
29. Gupta, C. S. 2003. The Classical Stefan Problem. Elsevier, New York.
30. Rubinshtein, L. I. 1971. The Stefan Problem. American Mathematical Society, Providence, RI.
31. Fung, Y. C. 1993. Biomechanics: Mechanical Properties of Living Tissues. Springer, New York.
32. Canetta, E., A. Duperray, …, C. Verdier. 2005. Measuring cell viscoelastic properties using a force-spectrometer: influence of protein-cytoplasm interactions. *Biorheology.* 42:321–333.
33. Hanzawa, E. 1981. Classical solutions of the Stefan problem. *Tohoku Math. J.* 33:297–335.
34. Kamenomostskaja, S. L. 1965. On the Stefan problem. *Mat. Sb.* 53:485–514.
35. Oleinik, O. A. 1960. On a method of the construction of solutions of the Stefan problem. *Dokl. Acad. Nauk USSR.* 135:1054–1057.
36. Friedman, A. 1968. The Stefan problem in several space variables. *Trans. Amer. Math. Soc.* 133:51–87.
37. Mullins, W. W., and R. F. Sekerka. 2009. Stability of a planar interface during solidification of a dilute binary alloy. *J. Appl. Phys.* 35:444–451.
38. Osher, S., and J. A. Sethian. 1988. Fronts propagating with curvature-dependent speed: algorithms based on Hamilton-Jacobi formulations. *J. Comput. Phys.* 79:12–49.
39. Chen, S., B. Merriman, …, P. Smereka. 1997. A simple level set method for solving Stefan problems. *J. Comput. Phys.* 135:8–29.
40. Javierre, E., C. Vuik, …, A. Segal. 2007. A level set method for three dimensional vector Stefan problems: dissolution of stoichiometric particles in multi-component alloys. *J. Comput. Phys.* 224:222–240.
41. du Roure, O., A. Saez, …, B. Ladoux. 2005. Force mapping in epithelial cell migration. *Proc. Natl. Acad. Sci. USA.* 102:2390–2395.
42. Callaghan, T., E. Khaih, …, R. M. Ziff. 2006. A stochastic model for wound healing. *J. Stat. Phys.* 122:909–924.